Molecular Microbiology (2012) 84(5), 874–891 ■
doi:10.1111/j.1365-2958.2012.08063.x
First published online 2 May 2012

Measuring the stiffness of bacterial cells from growth rates in hydrogels of tunable elasticity

Hannah H. Tuson,[1‡] George K. Auer,[2‡] Lars D. Renner,[1] Mariko Hasebe,[1] Carolina Tropini,[3] Max Salick,[4] Wendy C. Crone,[2,5] Ajay Gopinathan,[6] Kerwyn Casey Huang[3†] and Douglas B. Weibel[1,2*]

[1]*Department of Biochemistry, University of Wisconsin-Madison, 433 Babcock Drive, Madison, WI 53706, USA.*

[2]*Department of Biomedical Engineering, University of Wisconsin-Madison, 1550 Engineering Drive, Madison, WI 53706, USA.*

[3]*Department of Bioengineering, Stanford University, James Clark Center, 318 Campus Drive, Stanford, CA 94305, USA.*

[4]*Materials Science Program, University of Wisconsin-Madison, 1509 University Avenue, Madison, WI 53706, USA.*

[5]*Department of Engineering Physics, University of Wisconsin-Madison, 1500 Engineering Drive, Madison, WI 53706, USA.*

[6]*Physics and Chemistry Group, University of California-Merced, 5200 North Lake Road, Merced, CA 95343, USA.*

Summary

Although bacterial cells are known to experience large forces from osmotic pressure differences and their local microenvironment, quantitative measurements of the mechanical properties of *growing* bacterial cells have been limited. We provide an experimental approach and theoretical framework for measuring the mechanical properties of live bacteria. We encapsulated bacteria in agarose with a user-defined stiffness, measured the growth rate of individual cells and fit data to a thin-shell mechanical model to extract the effective longitudinal Young's modulus of the cell envelope of *Escherichia coli* (50–150 MPa), *Bacillus subtilis* (100–200 MPa) and *Pseudomonas aeruginosa* (100–200 MPa). Our data provide estimates of cell wall stiffness similar to values obtained via the more labour-intensive technique of atomic force microscopy. To address physiological perturbations that produce changes in cellular mechanical properties, we tested the effect of A22-induced MreB depolymerization on the stiffness of *E. coli*. The effective longitudinal Young's modulus was not significantly affected by A22 treatment at short time scales, supporting a model in which the interactions between MreB and the cell wall persist on the same time scale as growth. Our technique therefore enables the rapid determination of how changes in genotype and biochemistry affect the mechanical properties of the bacterial envelope.

Accepted 3 April, 2012. For correspondence. *E-mail weibel@biochem.wisc.edu; Tel. (+1) 608 890 1342; Fax (+1) 608 265 0764; †E-mail kchuang@stanford.edu; Tel. (+1) 650 721 2483; Fax (+1) 650 724 1922. ‡Authors contributed equally to this manuscript.

Introduction

The bacterial cell wall is a rigid network surrounding the cytoplasmic membrane that is required for cellular integrity and the maintenance of cell shape in virtually all eubacteria. The cell wall is composed of peptidoglycan, a macromolecule consisting of polysaccharides cross-linked by peptide bonds, and bears the stress of turgor pressures as high as 25 atmospheres to protect bacteria from osmotic shock and mechanical stress (Holtje, 1998; Vollmer and Bertsche, 2008). The cell wall is hydrated [~ 85% of the mass is bound water (Hobot *et al.*, 1984)], stiff, viscoelastic, and is the primary load-bearing material in both Gram-negative and Gram-positive bacteria (Xu *et al.*, 1996; Yao *et al.*, 1999).

Peptidoglycan synthesis, remodelling and regulation are central to bacterial physiology, with cell shape and size directly involved in a variety of critical functions including division, cell motility, cellular differentiation and immunity. A growing body of evidence suggests that cytoskeletal proteins control the spatial organization of peptidoglycan growth in replicating bacteria and participate in regulating the size and shape of cells. Electron cryotomography has revealed a common peptidoglycan ultrastructure in isolated, intact cell walls (sacculi) from *Escherichia coli* and *Caulobacter crescentus* with a single, 2 to 4 nm-thick layer of glycan strands that are preferentially oriented circumferentially around the cylindrical cell body (Gan *et al.*, 2008). In *Bacillus subtilis*, there is evidence that the glycan strands form cables that have an orientation similar to that in *E. coli* and *C. crescentus* (Hayhurst *et al.*, 2008).

Table 1. Young's modulus measurements for Gram-negative (pink) and Gram-positive (gray) bacteria.

Organism	Strain	*E* (MPa)	Conditions	Reference
E. coli	AB264	25	Isolated sacculi	Yao *et al.* (1999)
E. coli	JM109	12.8	Whole cells	Abu-Lail and Camesano (2006)
E. coli	JM109	0.12	Whole cells	Chen *et al.* (2009)
E. coli	JM109	0.05	Whole cells + EDTA	Chen *et al.* (2009)
E. coli	DH5α	2–3	Whole cells (live)	Cerf *et al.* (2009)
E. coli	DH5α	6	Whole cells (dead)	Cerf *et al.* (2009)
E. coli	NCTC 9001	221	Whole cells	Eaton *et al.* (2008)
E. coli	NCTC 9001	182	Whole cells + COS	Eaton *et al.* (2008)
E. coli	BE100	32	Whole cells	Deng *et al.* (2011)
E. coli	ATCC 9637	2.6	Whole cells	Perry *et al.* (2009)
S. paucimobilis	–	0.05	Whole cells	Penegar *et al.* (1999)
S. paucimobilis	–	0.08	Whole cells + Cu(II)	Penegar *et al.* (1999)
S. putrefaciens	CN32	0.21	Ph 4; force spectroscopy mode	Gaboriaud *et al.* (2005)
S. putrefaciens	CN32	0.04	Ph 10; force spectroscopy mode	Gaboriaud *et al.* (2005)
S. putrefaciens	CN32	69–98	Force volume mode	Gaboriaud *et al.* (2008)
S. aureus	NCTC 8532	95	Whole cells	Eaton *et al.* (2008)
S. aureus	NCTC 8532	88	Whole cells + COS	Eaton *et al.* (2008)
S. aureus	ATCC 25923	1.8	Whole cells	Francius *et al.* (2008)
S. aureus	ATCC 25923	0.2	Post-lysostaphin	Francius *et al.* (2008)
S. aureus	ATCC 25923	0.57	Whole cells	Perry *et al.* (2009)
B. subtilis	FJ7	10–30	Bacterial filament	Thwaites and Mendelson (1989; 1991), Thwaites and Surana (1991)
B. casei	–	769	Whole cells	Kumar *et al.* (2009)

Full species designations are *Escherichia coli*, *Sphingomonas paucimobilis*, *Shewanella putrefaciens*, *Staphylococcus aureus*, *Bacillus subtilis* and *Brevibacterium casei*.
COS, chitooligosaccharide; EDTA, ethylenediaminetetraacetic acid.

Theoretical models have provided a framework for inferring the molecular stiffness of the peptide cross-links from macroscopic measurements of the peptidoglycan Young's modulus (Boulbitch *et al.*, 2000) and determining the consequent effects on cell shape (Huang *et al.*, 2008; Furchtgott *et al.*, 2011).

Although peptidoglycan is widely conserved in bacteria, our understanding of its physical properties is limited to studies from a small number of model organisms, and it is unclear how pertinent these characteristics are across bacteria. The stiffness of a material can be described by the tensile elasticity or Young's modulus (E), which is measured in units of Pa (N m^{-2}) and represents the ratio between the applied stress on the material (force per unit area) and the resulting strain (fractional change in length). The Young's modulus is analogous to the force constant describing the restoring force exerted by a stretched spring: for a block of material of length L, the force F required to cause a fractional length change $\Delta L/L_0$ is $F = EA\Delta L/L_0$, where A is the area of the face onto which the force is applied. In principle, the Young's modulus can vary depending on the direction of the applied force; our analysis focuses on the modulus in the direction of growth: that is, along the long axis of the cell. For a thin shell similar to the cell wall of a rod-shaped bacterium in which the cross-sectional face is an annulus of thickness d, the force required for extension in the longitudinal direction increases linearly with d. A Gram-positive cell with a thicker wall (and thus a greater cross-sectional area) will require a larger force for its extension than a Gram-negative cell with a thinner wall. As a result, a Gram-positive cell will extend less at a given stress (such as that produced by turgor pressure) if the Young's modulus of the wall is the same as a Gram-negative cell. Representing the elastic properties of a material as a single value of the Young's modulus assumes a linear response (force linearly proportional to extension); a non-linear response can be translated into a range of values of the Young's modulus.

Tensile strength measurements and atomic force microscopy (AFM) are two methods that have been used to measure the Young's modulus for intact peptidoglycan fragments and for both live and dead bacterial cells. Using tensile strength measurements, Thwaites and Mendelson studied extruded filaments of cells from *B. subtilis* strain FJ7 (Δ*lyt*) and determined that the Young's modulus of the cells (E_{cell}) was ~ 30 MPa (Table 1) (Thwaites and Mendelson, 1989; 1991; Thwaites and Surana, 1991). Although this method is conceptually straightforward, an obvious disadvantage is that most bacterial strains do not form mesoscopic threads and hence are not compatible with this technique.

In a typical AFM experiment, cells are immobilized on a surface and imaged using contact or tapping mode AFM. Force curves are measured at various locations on the cell surface and are fit to a model of cell mechanics to

extract the Young's modulus. AFM has been used to measure E_{cell} for several Gram-positive and Gram-negative bacteria using force spectroscopy or force volume mode measurements, although reported values vary by several orders of magnitude, even for a single species (Table 1). Despite the quantitative nature of AFM, several technical challenges remain, most notably: (i) modulus measurements are typically restricted to a small area of the cell surface, which can lead to large standard deviations (Abu-Lail and Camesano, 2006), (ii) local deformations of the cell wall may be larger than the diameter of the probe (Vadillo-Rodriguez *et al.*, 2008), (iii) meticulous sample preparation, measurements and data analysis are required and (iv) the cost, throughput and availability of these instruments in microbiology labs is generally prohibitive. Therefore, a technique for the rapid screening of strains, mutants or environmental conditions that influence the mechanical properties of the cell wall *in vivo* will be critical for expanding the exploration of mechanical properties initiated by AFM studies.

Here we report a new technique for measuring the mechanical properties of bacterial cells *in vivo* that we refer to as Cell Length Analysis of Mechanical Properties (CLAMP). This methodology represents a first step in developing a high-throughput capability for measuring bacterial cell stiffness in a species-independent manner. As the cell envelope is a complex structure consisting of multiple materials, we refer to this stiffness as an effective Young's modulus (E_{cell}). CLAMP combines quantitative analysis of time-lapse imaging and biophysical modelling to enable the determination of E_{cell} using standard equipment found in microbiology labs. We encapsulated bacterial cells in layers of agarose with a user-defined stiffness (E_{gel}), determined the initial growth rates of individual cells in hydrogels of varying stiffness using phase contrast optical microscopy and fit the data to three-dimensional finite-element simulations to determine E_{cell}. The synthesis of biophysical theory and experiment has previously been successful in elucidating the mechanisms by which bacteria determine and maintain their shape (Huang *et al.*, 2008; Furchtgott *et al.*, 2011); here we employed modelling to establish a framework for interpreting CLAMP-derived imaging data.

We used CLAMP to measure and compare E_{cell} for *E. coli* MG1655, *Pseudomonas aeruginosa* PAO1 and *B. subtilis* BB11. Despite the differences in cell wall thickness among these species, our results suggest that the Young's modulus of the cell envelope is similar, indicating that these species may share a common network architecture. We also found that depolymerization of MreB using the small molecule A22 did not significantly affect the longitudinal stiffness of *E. coli* cells, illustrating the utility of CLAMP in the study of how physiological perturbations affect the mechanical properties of bacterial cells. CLAMP therefore provides an integrated experimental and computational platform that enables fundamental studies of the bacterial cell wall. We envision that this paradigm will become the foundation for physical studies of living cells.

Results

Experimental system for measuring cell elongation in hydrogels

We designed our experimental system (Fig. 1) to be a quantitative, reproducible assay that is capable of medium- or high-throughput analysis of cell stiffness. This approach is technically straightforward, incorporates components found in most biological labs and consists of an extendable platform that accommodates the assaying of cellular mechanical properties in a wide variety of bacteria and other organisms, including yeast and fungi. We used agarose as the polymer for encapsulating bacteria for several reasons, including: (i) it is biocompatible and has been used previously to encapsulate a variety of cell types, including bacteria (Katsuragi *et al.*, 2000; Zengler *et al.*, 2002; Eun *et al.*, 2011), (ii) it is chemically and mechanically stable and may be polymerized with user-defined stiffness spanning the kPa to MPa regime (Figs S1 and S2), (iii) it is relatively transparent to the diffusion of ions, small molecules, secondary metabolites and metabolic waste, and gases, which is an important feature for maintaining normal cell growth, (iv) it hydrates encapsulated cells, a critical factor impacting measurements of E_{cell} by AFM (Table 1) and (v) bacteria in contact with agarose continue to grow (Fig. S3).

We encapsulated cells in agarose layers and measured their growth using phase contrast microscopy and automated image analysis (Fig. 1). In a typical experiment we adjusted the imaging focal plane of the microscope so that it extended ~ 50 μm into the agarose from the top of the gel, thus avoiding issues of gas diffusion that could affect the growth of aerobic bacteria. We only measured and analysed the growth of bacterial cells that were separated by more than 5 μm from their closest neighbours to avoid mechanical interactions mediated by gel compression. For each species, we imaged the growth of ~ 30 cells at each concentration of agarose every 1 min for 30 min, a time frame selected based on their typical division times in liquid media. To increase the number of cells appearing in focus at each time point, we found that the gel could be optically sectioned by moving the *z*-axis of the gel in 500 nm increments and imaging cells in 10 different focal planes (Fig. 1).

Our initial experiments focused on *E. coli*, *B. subtilis* and *P. aeruginosa* because the mechanical properties of the bacterial cell wall have been most frequently examined in these organisms (Table 1). We systematically analysed the growth of cells encapsulated in 1–8% (w/v) agarose gels.

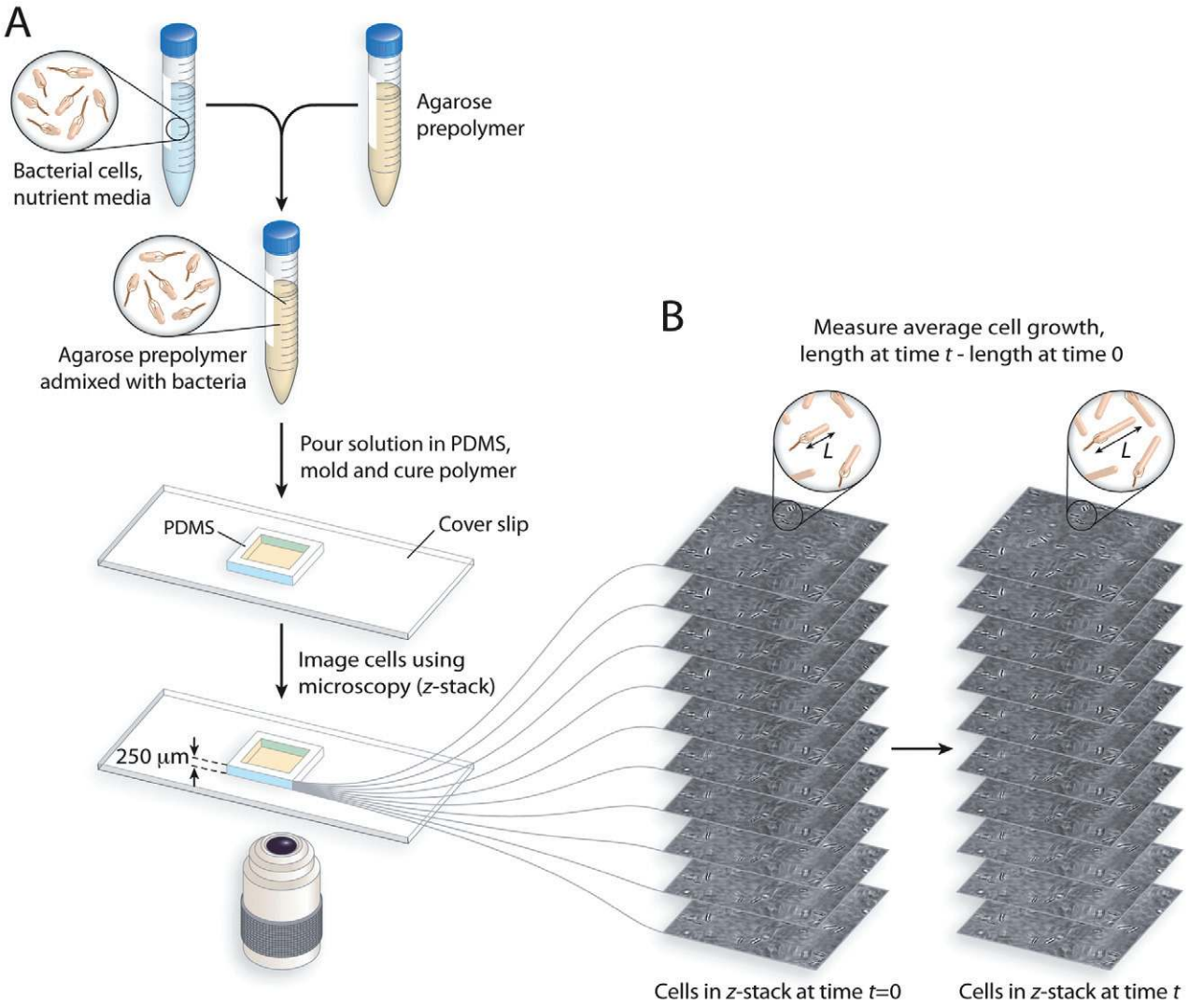

Fig. 1. Methodology for encapsulating bacterial cells in agarose gels and measuring their growth.
A. Cells are mixed with a warm agarose solution, poured into a polydimethylsiloxane (PDMS) chamber and gelled. The resulting agarose slab (15 mm on an edge, 250 μm tall) is mounted on a heated stage and imaged with phase contrast microscopy.
B. Cells are imaged in multiple focal planes (*z*-stack) at 1 min intervals to increase the number of cells for analysis. The cell length, *L*, is determined over time using image analysis scripts.

To characterize the mechanical properties of these gels, we measured E_{gel} for various agarose concentrations [infused with Luria–Bertani (LB) media, but without cells] using tensile testing with an Instron MicroTester. The modulus increased linearly with the agarose concentration over two orders of magnitude, with $E_{gel} \approx 60$ kPa for a 1% gel and 1500 kPa for an 8% gel (Fig. S1).

We found that cells elongated linearly in agarose gels at early time points. Relative cell elongation (the change in cell length divided by the initial cell length, $\Delta L/L_0$) reached saturation slowly when encapsulated in gels of low E_{gel} and more rapidly as E_{gel} was increased (Fig. 2). To ascertain whether the cells were still viable once cell length plateaued, we queried the metabolic state of encapsulated *E. coli* cells using the redox indicator 5-cyano 2,3-ditolyltetrazolium chloride. Encapsulated cells only slightly elongated after 90 min but nevertheless remained metabolically active (Fig. S4). To ascertain whether cellular uptake of small molecules was affected by gel strength, we measured the diffusion of fluorescein through 1% and 5% agarose gels. The mean distance of fluorescein diffusion in these gels was within the standard deviation of the measurements (Fig. S5), and thus we concluded that the decrease in growth rate for encapsulated cells was not due to nutrient diffusion. We therefore inferred that growth inhibition at increasing E_{gel} can be attributed to the compressive force imparted by the agarose, which resists the extension of the bacterial cell wall.

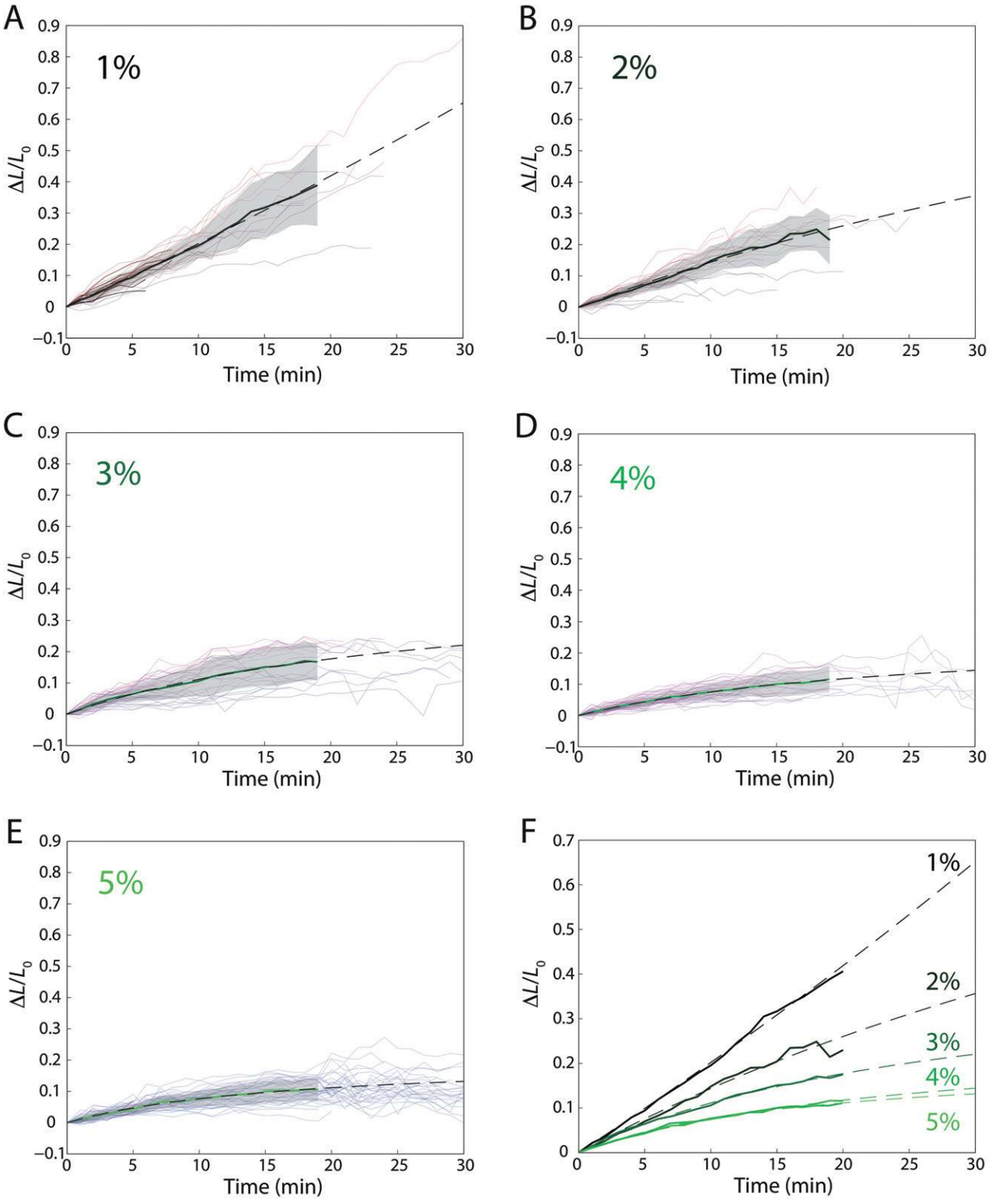

Fig. 2. Growth of *E. coli* MG1655 cells saturates when cells are embedded in stiff agarose gels.
A–E. Growth curves of individual cells embedded in 1–5% agarose gels ($n \geq 26$ cells for each agarose concentration). Solid thick lines represent the average growth curve of all cells at a given agarose concentration, while shaded areas indicate one standard deviation above and below the mean growth curves.
F. Compilation of average growth data from A–E at all agarose concentrations. Dashed lines are fits to Eq. 5 of the average growth during the first 20 min (black to green gradient denotes increasing agarose concentration and therefore increasing gel stiffness).

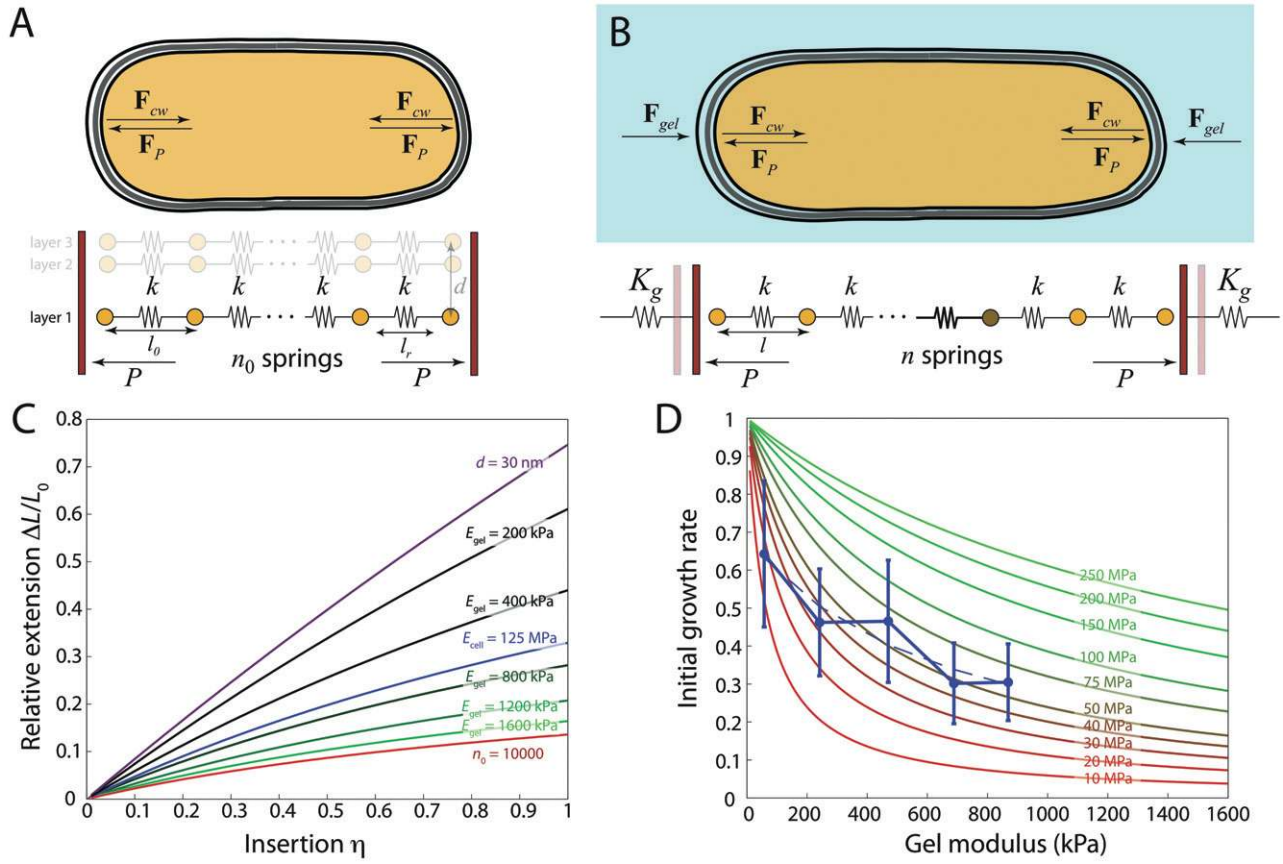

Fig. 3. Gel inhibition of cell growth predicted by a one-dimensional spring model.
A. A rod-shaped bacterial cell is modelled as a connected line of n_0 springs each with spring constant k and relaxed spring length l_r, with pressure P exerting a force on the cell ends (red rectangles) that extends the length of the springs to l_0. Initially, the turgor (F_P) and spring extension forces (F_{cw}) are balanced. A multilayer cell wall with thickness d is modelled as multiple lines of springs.
B. As the agarose-encapsulated cell grows to a length of n springs in a gel modelled by a spring constant K_g, full elongation (light red rectangles) is inhibited by the restoring force of the gel (F_{gel}). The newly inserted vertex and spring appear brown and in bold respectively.
C. Relative elongation $\Delta L/L_0$ as a function of the fractional insertion $\eta = \Delta n/n_0$ for different values of the stiffness ratio $\xi = kd/n_0K_g$. Cell growth becomes increasingly inhibited as the gel modulus K_g increases (black to green gradient of curves, with $E_{cell} = 100$ MPa, $d = 4$ nm, $n_0 = 4000$). For a fixed gel modulus of 800 kPa, the growth is more inhibited for longer cells ($n_0 = 10\,000$, red curve) and less inhibited for stiffer cells ($E_{cell} = 125$ MPa, blue curve) or thicker cell walls ($d = 30$ nm, purple curve).
D. Predictions of initial growth rate $d(\Delta L/L_0)/d\eta$ for different values of the cell modulus E_{cell} based on our one-dimensional model. Our experimental measurements of initial growth rate for *E. coli* MG1655 cells (blue circles) fall between 20 and 75 MPa. Error bars indicate one standard deviation about the mean. The dashed line is a fit to Eq. 4.

Analytical model of elongation in an elastic hydrogel

To provide a framework for interpreting our data on cell growth in elastic gels, we first present a simple one-dimensional model of an elastic rod-shaped bacterial cell that predicts the qualitative growth dynamics in our experiments. We modelled the cell wall as a connected chain of n_0 springs each with spring constant k and relaxed length l_r; we use lowercase l to denote the length of a single spring and uppercase L to denote the length of the cell (Fig. 3A). Each spring represents a longitudinally oriented peptide cross-link within the cell wall. For a cell wall with thickness d and radius r, k is related to the longitudinal Young's modulus E_{cell} via the relation $k = 2\pi rdE_{cell}/l_r$. Since the springs are arranged in series, their combined mechanical response to an applied force is equivalent to that of a single spring with a smaller effective spring constant $K_0 = k/n_0$ and longer relaxed length $L_{0r} = n_0l_r$. Before the cell is embedded in the gel, the only longitudinal force across the wall arises from turgor pressure P acting on the cell ends, which extends the combined length of the springs to a total length L_0. Assuming that the cell is at mechanical equilibrium, each spring extends to a length l_0 and force balance dictates that $P = K_0(L_0 - L_{0r})$ where $L_0 = n_0l_0$.

Once the cell is embedded in a gel, we assume that the major forces in the gel are compressive along the longitudinal axis due to cell growth. Thus, we represent the surrounding material as a spring with force constant K_g and model cell growth by inserting material to reach a new length of n springs ($n > n_0$) so that the cell will extend to

length $L = nl$ (Fig. 3B). The length of each spring after growth (l) is a function of K_g and n and is less than the expected length l_0 that would occur in liquid, due to the restoring force of the gel as the cell attempts to displace the gel. Equivalently, one can think of the gel as relieving some of the force due to turgor pressure, which then reduces the extension of the springs. We can estimate K_g from E_{gel} by assuming that the force is evenly distributed within the gel over a length scale λ that is similar to the micron size of the cell, such that $K_g \approx E_{gel}\lambda$. For $E_{gel} = 1$ MPa and $\lambda = 1$ μm, the equivalent spring constant is $K_g = 1000$ pN nm^{-1}. Balancing the force due to turgor pressure with the forces due to gel compression and cell extension,

$$P = K_g(L - L_0) + \frac{k}{n}(L - nl_0^r). \quad (1)$$

For the case $L = L_0$ and $n = n_0$, Eq. 1 gives $P = k(l_0 - l_0^r)$, which allows us to eliminate the variable P from the relative elongation of the cell. By balancing the compressive force of the gel with the expansion force of the cell due to growth (Fig. 3B), we find that,

$$K_g(L - L_0) = k(l_0 - l). \quad (2)$$

To compare theory and experiment, we solved for the fractional extension in our model,

$$\frac{\Delta L}{L_0} = \frac{\eta\xi}{\eta + 1 + \xi}, \quad (3)$$

where $\Delta L = L - L_0$, $\eta = \Delta n/n_0$ is the fractional insertion, and $\xi = k/n_0K_g$ is the ratio of the cellular and gel spring constants. Pressure does not appear on the right-hand side of Eq. 3, which is in agreement with a key prediction of our model: that is, the fractional extension ($\Delta L/L_0$) should be independent of turgor pressure, which contributes equally to ΔL and to L_0 and hence cancels from the ratio. $\Delta L/L_0$ has a sigmoidal shape as a function of η that is qualitatively similar to our experimental measurements in Fig. 2, with a growth saturation crossover point at $\eta = 1 + \xi$ (Fig. 3C). Our model predicts that some growth will occur even at high gel stiffness because there is initially little energy cost to compress the gel. Indeed, we observe that the growth rate of *E. coli* cells decreases but remains non-zero even in 5% agarose gels with stiffness of ~ 1 MPa (Fig. 2E).

Although our model does not depend on where the new material is inserted in the cell wall, connecting the fractional insertion and the insertion rate over time requires assumptions regarding the dependence of insertion on applied force. The external force from gel compression can stall the peptidoglycan synthesis machinery if a certain amount of extension is required, for example, to make room for newly inserted material. However, stall effects will be less important at early time points after encapsulation since little gel compression will have taken place. Moreover, if the force applied by the peptidoglycan synthesis machinery during insertion is large enough compared with the force of gel compression such that stalling can be ignored, then insertion will be unaffected by the confinement of the cells in the gel and the relative insertion η will be approximately linear in time.

As cells continue to insert peptidoglycan, the resulting network will become increasingly compressed, and the cell length will saturate at $L_{max} = L_0(1 + \xi)$; as the cell approaches this length, the gel compression increases to the point that the addition of new material results mostly in compression of the old material rather than elongation and further compression of the gel. In this scenario, our model predicts that the maximal relative extension $(L_{max} - L_0)/L_0$ will scale inversely with the gel modulus (proportional to $1/K_g$), independent of initial length.

A number of testable predictions follow immediately from Eq. 3. First, assuming that the gel stiffness K_g is a function only of the cross-sectional dimensions of the cell and hence is independent of n_0, the fractional increases in length and initial elongation rate should depend directly on the initial cell length (which is proportional to n_0); since longer cells require more compression of the gel to achieve a given fractional elongation, they will grow more slowly and saturate at a shorter fractional extension. Second, $\Delta L/L_0$ should be invariant to an equal scaling of k and K_g, and thus two cells that differ in stiffness by the ratio k_1/k_2 should grow similarly if embedded in hydrogels with the same ratio of stiffness. The cell stiffness may change either by constructing peptidoglycan with a different architecture or by varying the thickness of the cell wall; we expect that for the same Young's modulus, the stiffness will increase linearly with the thickness. Using a relaxed peptide length $l_r = 1$ nm, Fig. 3C illustrates several predicted growth curves as a function of η for different values of the initial cell length (n_0) and the longitudinal Young's moduli of the cell and the gel. The curves representing the same cell in gels of different stiffness (green) are qualitatively similar to the growth curves in Fig. 2F, with a decrease in growth as the gel stiffness increases.

Our theory predicts the growth kinetics of cells with a given value of the surface modulus dE_{cell} (cell wall thickness multiplied by the Young's modulus) since the energy of the cell depends only on this product (Minc *et al.*, 2009). Thus, for testing an uncharacterized bacterium with CLAMP, a determination of the longitudinal Young's modulus obtained from growth kinetics similar to Fig. 3 requires an independent estimate of the cell wall thickness. Recent cryo-electron microscopy measurements have placed the cell wall thickness of the Gram-negative bacteria *E. coli* and *C. crescentus* at 2 to 4 nm (Gan *et al.*, 2008), suggesting that this may be a reasonable estimate for many Gram-negative cells. The thickness of the cell wall of the Gram-positive bacterium

B. subtilis has been estimated at ~ 30 nm (Thwaites and Surana, 1991; Matias and Beveridge, 2005; 2008).

The initial elongation rate near $\eta = 0$ calculated from Eq. 3 is predicted to also depend on k, n_0 and K_g and can be modelled by,

$$\left.\frac{d(\Delta L/L_0)}{d\eta}\right|_{\eta=0} = \frac{\xi}{1+\xi}. \quad (4)$$

Using Eq. 4, we produced a set of curves representing the growth of 4 μm cells with a wall thickness of 4 nm, a radius of 500 nm and different Young's moduli that can be directly compared with our experimental data in Fig. 2. To compare to experimental values, we measured the growth rate of *E. coli* cells in liquid in a microfluidic flow chamber (doubling time 23.7 ± 3.5 min, see *Experimental procedures* and Fig. S6A), which we assume closely mimics an unencapsulated growth environment and establishes the time scale for the synthesis and insertion of a given amount of material. The blue circles in Fig. 3D are experimental measurements derived from a linear fit to the first 5 min of *E. coli* MG1655 cell growth data at each agarose concentration in Fig. 2, normalized to the microfluidic chamber growth rate. Our experimental measurements fall between the curves representing cells with longitudinal Young's moduli of 20 to 75 MPa, with the data at larger agarose concentrations falling between 50 and 75 MPa (Fig. 3D). The range of possible Young's modulus values that are consistent with our data could represent a nonlinear response of the cell wall, or systematic experimental measurement errors. Nevertheless, the qualitative agreement between our model predictions and experimental measurements suggests that our model accurately represents the mechanical perturbations to the cell caused by gels of known stiffness, and provides an estimate for the stiffness of the cell wall.

Finite-element modelling of the bacterial cell wall as a thin shell

Although our one-dimensional model accurately predicts the qualitative behaviour of bacterial cells encapsulated in gels, a quantitative determination of the Young's modulus of the cell requires an accurate three-dimensional model of the cell geometry. To illustrate this point, there are two regions of the gel that have different responses depending on the initial cell length: the gel longitudinally compresses parallel to the long axis of the cell next to the endcaps, but also stretches adjacent to the cell body. The former compression is independent of L_0, but the latter stretching should scale with $1/L_0$, similar to the spring constant of the cell. Thus, to quantitatively predict the elastic properties of the cell, it was necessary to account for the geometric details of gel compression.

We modelled the cell envelope as a cylindrical thin shell with hemispherical endcaps whose deformation energy arises from bending, stretching and turgor forces. The gel is represented as a collection of connected small volumes with an isotropic Young's modulus whose compression energy was computed using a finite-element method (Zienkewicz, 2005). We simulated growth by increasing the relaxed length of the cylindrical portion of the cell by a fraction f, thereby increasing the energy of the cell due to longitudinal compression, and allowed the cell to relax mechanically by displacing the surrounding gel (see *Computational methods* in *Experimental procedures*). We assumed that during the early stages of growth in which $\Delta L \approx 0$, the insertion of new material is unlikely to be inhibited by the surrounding gel; therefore, we focused only on the cell deformation for small f and constant insertion rate, such that the fractional insertion η is linear in time t.

Based on estimates from our one-dimensional model, we computed the strain after 1% elongation in cell walls with an initial length of 4 μm, E_{cell} = 250 MPa, and cell wall thickness d = 4 nm embedded in a gel with E_{gel} = 56 kPa (Fig. 4A). The strain is clearly localized to a region of the gel within a few microns of the cell body (Fig. 4A), validating both our selection of individual cells for analysis that were > 5 μm from other cells encapsulated in the hydrogel and our estimate of K_g in our one-dimensional model. Next, we determined the relative rate of elongation of the embedded cell $d(\Delta L/L_0)/d\eta$ after 1% insertion as a function of E_{gel} for cells with various values of E_{cell} (Fig. 4B). To compare to experimental values, we normalized our measurements of the initial fractional elongation rate to the experimental time scale required for 1% insertion determined from the growth rate in a microfluidic flow chamber (Fig. S6A). To address the stiffness of Gram-positive cells, we also computed the gel stresses (Fig. 4C) and relative rate of elongation (Fig. 4D) for a cell wall with thickness 30 nm and length 8 μm. The increase in thickness more than offsets the decrease in effective stiffness due to increased cell length, leading to faster fractional elongation for a given gel modulus. In Fig. 4B and D, the qualitative behaviour is similar to the predictions of our one-dimensional model in which cell elongation increases with increasing E_{cell} and decreasing E_{gel}. The data in Fig. 4B and D can thus be considered a set of standard curves to which experimental measurements of the initial elongation rate can be fit to determine the most likely longitudinal Young's modulus of a given species within the assumptions of our model.

CLAMP predicts similar Young's moduli for different bacterial species

Growth curves for individual cells of *E. coli* MG1655 (Fig. 2), *P. aeruginosa* PAO1 (Fig. 5A) and *B. subtilis* BB11

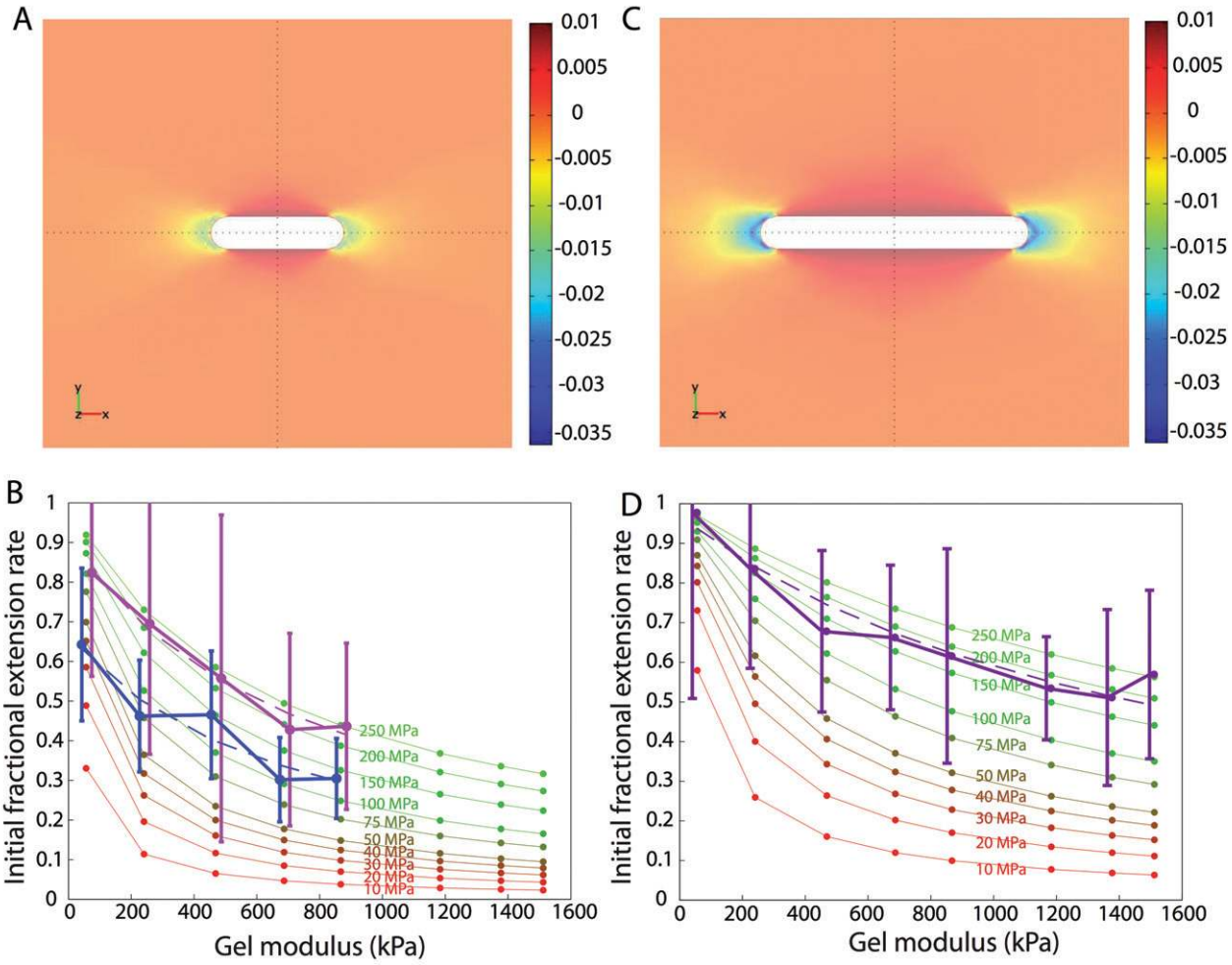

Fig. 4. Estimation of cellular mechanical properties based on three-dimensional simulations of growth.
A and C. Three-dimensional finite-element simulations of the mechanical equilibrium of a rod-shaped bacterium with a radius of 0.5 μm, cell wall thickness of 4 nm (A) or 30 nm (C), and Young's modulus $E_{cell} = 250$ MPa, embedded in a gel with $E_{gel} = 56$ kPa. Strains in the gel along the longitudinal axis of the cell (heat map) are depicted for cells with initial lengths of 4 μm (A) or 8 μm (C) after 1% growth of the cylindrical, mid-cell region.
B. Initial fractional extension rate $d(\Delta L/L_0)/d\eta$ from simulations of cells with different Young's moduli, initial length 4 μm, and envelope thickness 4 nm, after insertion of $\eta = 1\%$ new material. Close agreement between simulations and experimental measurements of initial fractional extension rates for *E. coli* MG1655 cells (blue) and *P. aeruginosa* PAO1 cells (magenta) predicts that $E_{cell} \approx 50$–150 MPa for *E. coli* and 100–200 MPa for *P. aeruginosa*. Error bars indicate one standard deviation about the mean; dashed lines are fits to Eq. 4.
D. Initial fractional extension rate $d(\Delta L/L_0)/d\eta$ from simulations of cells with different Young's moduli, initial length 8 μm, and envelope thickness 30 nm, after insertion of $\eta = 1\%$ new material. Close agreement between simulations and experimental measurements of initial fractional extension rates for *B. subtilis* BB11 cells (purple) predicts that $E_{cell} \approx 100$–200 MPa. Error bars indicate one standard deviation about the mean; dashed lines are fits to Eq. 4.
Experimental data in B and D is shown slightly offset for comparison with simulation data.

(Fig. 5B) grown in agarose with different values of E_{gel} fit well to the functional form,

$$\frac{L(t) - L_0}{L_0} = \frac{At}{t_{1/2} + t}, \tag{5}$$

which is similar to the predicted behaviour in our one-dimensional model (Eq. 3). We observed a similar degree of heterogeneity in the growth kinetics of individual cells encapsulated in gels and growing in microfluidic flow cells (Figs 2 and S6). In each case the single-cell growth curves were reasonably smooth and enabled us to extract the average initial growth rates in each gel and compare them to the predictions of our three-dimensional simulations (Fig. 4). To do so, we also measured the doubling times in liquid of *P. aeruginosa* PAO1 cells (31.8 ± 5.3 min, Fig. S6C) and *B. subtilis* BB11 (28.8 ± 7.1 min, Fig. S6D). Given the similarities between *P. aeruginosa* and *E. coli* (23.7 ± 3.5 min) doubling times and gel-encapsulated

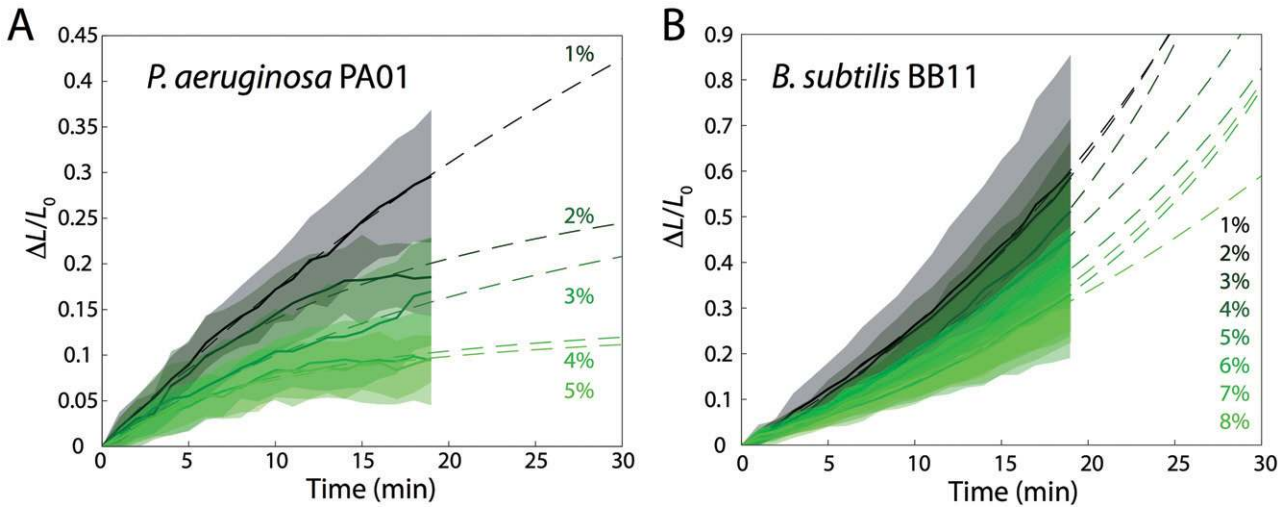

Fig. 5. Gram-negative and Gram-positive species both exhibit growth inhibition upon encapsulation. Average growth curves (solid lines) of (A) *P. aeruginosa* PAO1 and (B) *B. subtilis* BB11 cells embedded in agarose gels of various stiffnesses ($n \geq 27$ cells of *P. aeruginosa* PAO1 and $n \geq 17$ cells of *B. subtilis* BB11 for all agarose concentrations; black to green gradient denotes increasing agarose concentration and therefore increasing gel stiffness). Dashed lines are fits to Eq. 5 of growth during the first 20 min. Shaded regions indicate one standard deviation above and below the mean growth curves.

growth curves (Figs 2F and 5A), if we assume a similar wall thickness, our simulations predict similar values of the longitudinal Young's modulus for both species (50–150 MPa for *E. coli* and 100–200 MPa for *P. aeruginosa*, Fig. 4B).

Our models predict that growth should be more inhibited for longer cells at the same gel stiffness. To test this prediction we used *B. subtilis* strain BB11 in which a single copy of *ftsZ*, a gene that encodes an essential division protein, is placed under IPTG control at the chromosomal locus; these cells form filaments in the absence of IPTG. We removed IPTG and incubated *B. subtilis* BB11 to promote modest filamentation, and then measured the growth of cells encapsulated in 1% to 8% agarose gels. We binned cells based on whether their starting length was shorter than 9 μm or longer than 12 μm, and analysed their growth rates. As predicted, cell elongation was more inhibited for longer cells in gels of a given agarose concentration (Fig. S7). For gels at low agarose concentrations, *B. subtilis* BB11 growth curves exhibited an upward curvature at longer time scales. This increase in growth rate may arise from the tearing of the gel at high strains (~ 15%, Fig. S2). Regardless, this behaviour is unlikely to skew our determination of cell stiffness, since we use only data from the first 5 min of encapsulated growth – when strain in the gel is still within the linear, elastic regime (Fig. S2) – to calculate the initial growth rate. Assuming a cell wall thickness of 30 nm, our simulations predict that the longitudinal Young's modulus of *B. subtilis* BB11 cells is ~ 100–200 MPa (Fig. 4D).

Quantifying the role of MreB in cell mechanics

To demonstrate the utility of CLAMP for determining whether a change in stiffness occurs after a physiological perturbation, we focused on the role of the cytoskeleton in determining the stiffness of *E. coli* cells. MreB, a prokaryotic homologue of eukaryotic actin, is essential for maintaining a rod-like shape in bacteria such as *E. coli*, *B. subtilis* and *P. aeruginosa* (Gitai *et al.*, 2004; Kruse *et al.*, 2005; Carballido-Lopez and Formstone, 2007). MreB is thought to form oligomers or short filaments that are depolymerized by the small molecule inhibitor S-(3,4-dichlorobenzyl)isothiourea (A22) (Iwai *et al.*, 2002; Gitai *et al.*, 2005; Bean *et al.*, 2009). Using optical trapping, it was recently shown that the flexural (bending) rigidity of *E. coli* cells is reversibly reduced approximately twofold by A22 treatment (Wang *et al.*, 2010). This reduction in bending rigidity supports a model in which MreB is bound to the cell wall through the inner membrane and thereby influences the bending modulus of cells.

We used CLAMP to explore a different mechanical perturbation, in which the extension of the cell wall during *growth* is balanced by gel compression. Any significant contribution of MreB to the longitudinal stiffness of the cell would require it to remain bound to the cell wall on time scales significantly longer than growth; however, fluorescence recovery after photobleaching experiments of MreB filaments indicate rapid turnover (Defeu Soufo *et al.*, 2010). We used CLAMP to test the relationship between A22-induced disassembly of MreB filaments *in vivo* and longitudinal cell stiffness. We first

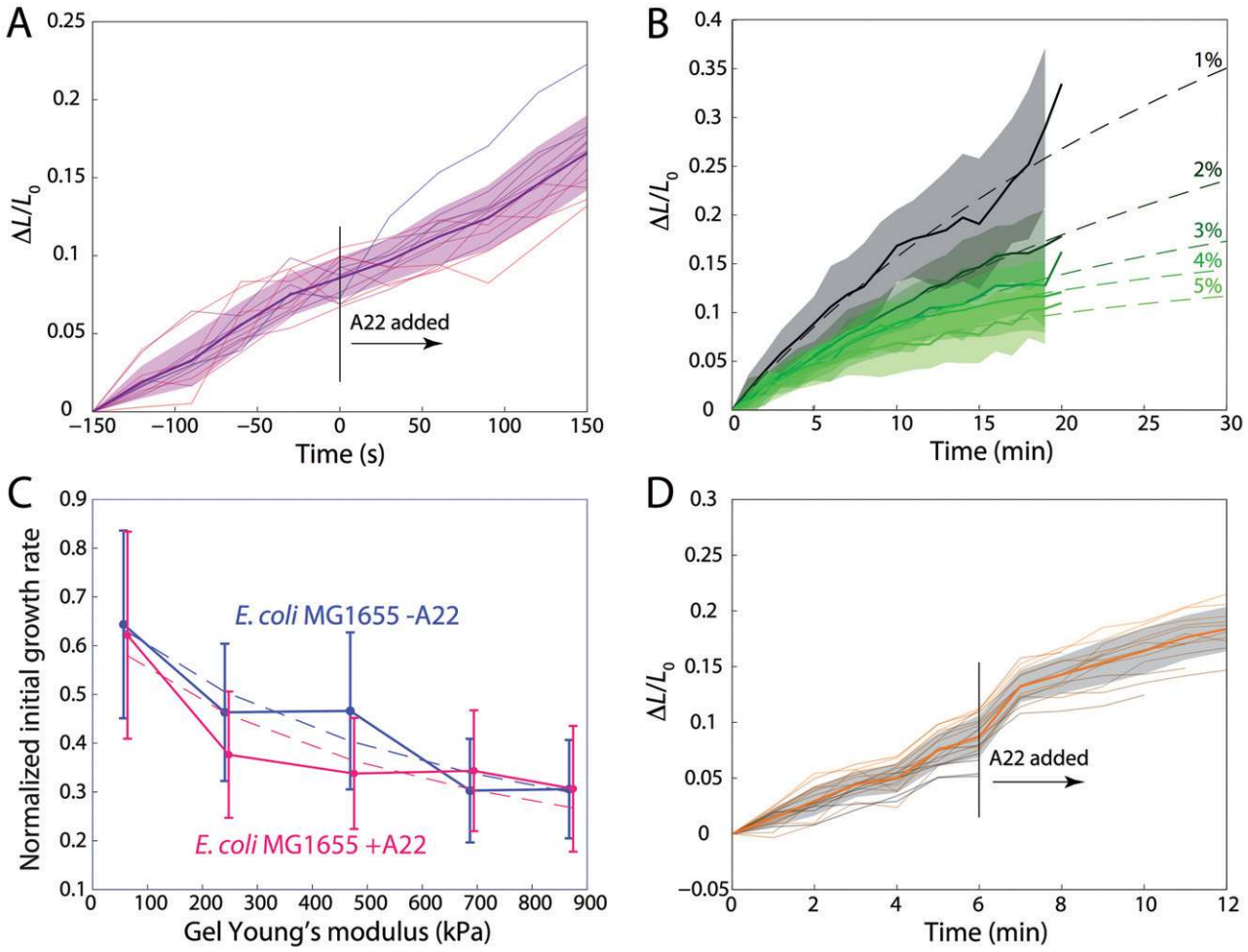

Fig. 6. A22 treatment does not reduce the longitudinal stiffness of growing *E. coli* cells.
A. Growth rate of individual *E. coli* cells ($n = 13$) in a microfluidic flow chamber is not affected by A22 treatment at $t = 0$.
B. Average growth curves (solid lines) for cells embedded in 1–5% agarose gels ($n \geq 24$ cells for each agarose concentration); black to green gradient denotes increasing agarose concentration and therefore increasing gel stiffness. Dashed lines are fits to Eq. 5 of growth during the first 20 min.
C. The average initial fractional extension rate during the first 5 min of growth is shown for cells with (pink) and without (blue) A22 as a function of increasing agarose stiffness. Liquid growth rate without A22 was used to normalize both curves. Error bars represent one standard deviation above and below the mean. Dashed lines represent fits to Eq. 4.
D. Average growth curve (solid line) for cells embedded in a 3% agarose gel ($n \geq 9$). A22 was added to the gel after 6 min of growth.
Shaded regions in A, B and D indicate one standard deviation above and below the mean growth curves.

measured the doubling time in a microfluidic flow chamber of *E. coli* MG1655 cells in LB containing A22 (10 μg ml^{-1}) to establish its effect on growth rate in the absence of mechanical stress. We found that inhibition of MreB by A22 did not affect the growth rate of *E. coli* MG1655 cells within the error of our growth rate measurements (22.3 ± 4.1 min, Fig. S6C), and there was no noticeable change in the growth of individual cells upon A22 addition (Fig. 6A). We then encapsulated *E. coli* MG1655 cells in agarose gels of varying stiffness containing 10 μg ml^{-1} A22 and immediately measured cell elongation at 1 min intervals (Fig. 6B). MreB was depolymerized by the time we started imaging (Fig. S8), and cells maintained their rod shape during the 30 min imaging time frame. Our measurements of agarose-embedded cells indicated that A22 treatment caused only a slight reduction in the initial fractional elongation rate (Fig. 6C) that was well within the error bars of our measurements, in quantitative agreement with the maintenance of growth rate of unencapsulated cells; we note that A22 treatment did cause a more dramatic ~ 30–50% reduction in the fractional elongation after 30 min (Fig. 6B). These data suggest that MreB alone has no effect on the longitudinal stiffness of actively growing *E. coli* cells, although growth in the absence of MreB may reduce cell wall stiffness.

As a further test, we realized that if MreB altered the longitudinal stiffness of the cell wall during growth, A22 treatment should reduce the amount of extensive force the cell is able to produce to displace the gel. For cells growing in agarose after sufficiently long time scales, treatment with A22 would then rapidly reduce cell length due to the force exerted on the cell by compression of the gel. Six minutes after encapsulating *E. coli* MG1655 cells within a 3% w/v agarose gel, we added a solution of A22 to the surface of the gel that after diffusion would produce a final A22 concentration of 10 $\mu g\ ml^{-1}$ within the gel, which is larger than the concentration required for MreB depolymerization. We imaged the cells throughout this procedure and found no detectable reduction in the length or growth rate of the cells after A22 treatment (Fig. 6D). Taken together, these observations indicate that MreB does not affect the longitudinal Young's modulus of the cell envelope during growth, and that MreB is bound to the cell wall in an unstressed state such that its depolymerization does not alter the mechanical equilibrium between cell wall extension and turgor forces.

Discussion

Here we describe an integrated computational and experimental approach for measuring the longitudinal stiffness of live, intact bacteria (Fig. 1). Cell growth was inhibited by encapsulation in stiff agarose gels (Fig. 2) in which the cells remained metabolically active (Fig. S4). Previous studies have demonstrated the long-term survival of bacterial cells encapsulated in rigid materials (Flemming *et al*., 1994; Young *et al*., 2006), with one study showing that cells of *Azospirillum brasilense* and *Pseudomonas fluorescens* are viable even after 14 years of encapsulation in alginate (Bashan and Gonzalez, 1999). We used CLAMP to determine E_{cell} for the rod-shaped bacteria *E. coli*, *B. subtilis* and *P. aeruginosa* (Figs 4 and 5) and thereby laid the groundwork for studying a wide range of other bacteria. Our simple, one-dimensional biophysical model for the elongation of rod-shaped cells embedded in gels predicts all of the qualitative features of our experiments (Fig. 3), and our three-dimensional finite-element simulations make possible quantitative comparisons with experimental data (Fig. 4).

Our measurements indicate a range of Young's modulus values for *E. coli* cells that is three to fivefold higher than some AFM measurements of isolated cell walls (Yao *et al*., 1999; Deng *et al*., 2011), although the large spread of AFM data for *E. coli* in the literature suggests that these measurements are extremely sensitive to environmental conditions. In contrast to many AFM measurements, our measurements specifically address the stiffness of live, growing cells, which may be different from isolated cell walls; for instance, the outer membrane of Gram-negative cells may also contribute to stiffness such that our measurements actually probe the combined stiffness of the cell envelope. It is also possible that the high values of E_{cell} that we have inferred are inflated due to incomplete polymerization of the gel around the cell (leading us to assume a higher gel modulus around the cell than is actually the case). While this point is difficult to address experimentally, it should not significantly affect our ability to measure relative changes in stiffness due to perturbations such as A22 treatment as long as the polymerization reaches similar levels of completeness at all gel concentrations. In fact, independent of the model used to infer cellular stiffness, our method can be utilized to determine the ratio of the stiffness of two strains of the same species or in media containing antibiotics or other biologically active small molecules by simply comparing fractional elongation rates.

Using the inhibitor A22 to rapidly depolymerize MreB, we demonstrated that MreB likely does not affect the longitudinal stiffness of the *E. coli* cell wall during growth; MreB disassembly had little effect on either the unencapsulated growth rate (Fig. S6B) or the encapsulated growth rate (Fig. 6) relative to untreated cells. These results demonstrate the quantitative nature of our methodology: despite cell-to-cell variation in single-cell growth rates, we observed the same A22 independence of growth rates in microfluidic flow chambers and in agarose gels across a wide range of values of stiffness. We note that our data do not contradict previous observations of MreB increasing the bending rigidity of *E. coli* cells (Wang *et al*., 2010), which predict that a similar reduction in stiffness should be observed if forces unrelated to growth are exerted to shorten or elongate A22-treated cells. Instead, our observations probed a different scenario of growth-related elongation due to cell wall insertion. The impact of MreB on bending stiffness but not longitudinal stiffness during elongation requires MreB to form rigid polymers whose dynamics are comparable with cell wall insertion. Indeed, recent studies have shown that MreB rotates in a circumferential direction driven by cell wall synthesis (van Teeffelen *et al*., 2011), and that MreB is only transiently attached to the cell wall and does not stretch as it mediates cell wall insertion, but rather unbinds and moves along the cell wall to the next position of cell wall assembly. CLAMP studies of A22 treatment of other bacterial species may help elucidate the relationship between MreB dynamics and cell wall insertion.

Our analysis has assumed linear springs; although we cannot rule out non-linear effects resulting from forces due to turgor pressure or gel compression, our method for longitudinal Young's modulus determination utilizes growth data only from the first few minutes after encapsulation, during which gel compression is small. Although our model does not enable us to distinguish between stiffness arising

from the thickness of the cell wall versus stiffness resulting from a material with a larger Young's modulus (Fig. 3C), our methodology generates a direct estimate for the cellular stiffness of a living bacterium. The reasonable agreement between the cellular Young's modulus determined by our measurements (Fig. 4B and D) and data from AFM experiments on isolated sacculi (Table 1) indicate that the cell wall is the major contributor to stiffness, as has been previously hypothesized. Given that the cell wall thicknesses of various Gram-negative bacteria are hypothesized to be similar (Gan *et al*., 2008), our observation that the growth of encapsulated Gram-negative cells of *E. coli* and *P. aeruginosa* is slowed at a similar value of E_{gel} (Figs 2 and 5) suggests that Gram-negative peptidoglycan is a material with common mechanical properties across species. This characteristic of peptidoglycan has important consequences for molecular-level modelling of the organization of Gram-negative peptidoglycan, and obviates the need for species-specific parameters representing peptide cross-link stiffness (Huang *et al*., 2008; Wang *et al*., 2010; Furchtgott *et al*., 2011).

There are a number of advantages to our technique. CLAMP is rapid, conceptually simple, easy to implement, and employs materials that are found in most biological laboratories. The development of a computational model for analysing the growth kinetics of new bacteria is rapid and depends only on the initial shape of the cell and a model for the location of newly inserted cell wall precursors. In addition to rod-shaped bacteria, cells with other shapes can also be analysed with CLAMP. Since agarose is compatible with the encapsulation of a variety of other organisms, it should be possible to extend this technique to the measurement of yeast (Gift *et al*., 1996), fungi (Jain *et al*., 2010) and Archaea (Ben-Dov *et al*., 2009). In principle, other biologically compatible hydrogels can be used as long as they are sufficiently stiff and are physically unchanged in the presence of ions and biomolecules secreted by encapsulated bacteria. Although experimentally untested, it should be possible to measure E_{cell} for different species simultaneously by mixing them together in the same gel, as long as the cells can be cultured in a single medium and have distinguishing features such as species-specific fluorescence or different cell morphologies.

Several aspects of this technique can be improved. CLAMP requires measurable cell growth over the time scale of an experiment, which places limitations on the time scale for determining the Young's moduli of slow-growing bacteria. At present the technique lacks the resolution of force volume and force spectroscopy AFM measurements, although this may be a result of heterogeneity in growth dynamics between cells. Here we have reported the growth rate of cells in agarose gels that vary by 1% (w/v) concentration changes; it is possible to make gels reproducibly that vary by smaller increments. The resolution of CLAMP may be improved by measuring cell growth at smaller increments of gel concentration, possibly increasing the accuracy of determining the growth-inhibiting gel concentration. CLAMP is ultimately limited by the resolution of optical microscopy, which makes it difficult to detect very small changes in cell length. One approach for improving the resolution is to incorporate fluorescent nanoparticles into the gel as tracers before polymerization and employ traction force microscopy to measure the displacement of the particles by the cells (Wang and Lin, 2007; Sabass *et al*., 2008).

There are a variety of interesting structural questions that CLAMP is particularly well suited to probe in bacteria. For example, CLAMP will enable studies of the mechanical properties of bacterial cells in the context of antimicrobial technologies. β-Lactams are the most successful family of antibiotics to date, targeting the enzymes that assemble and remodel the peptidoglycan. These small molecules are suicide inhibitors of the penicillin-binding proteins that play a role in peptidoglycan synthesis during cell replication (Popham and Young, 2003). Inhibition of the penicillin-binding proteins produces defects in the cell wall and leads to changes in cell shape and size and eventually to lysis (Nilsen *et al*., 2004; Varma and Young, 2004). Although the β-lactams have been mainstays in the arsenal of antimicrobial compounds since the 1940s, the resistance of bacteria to these compounds has slowly reduced their impact in the treatment of infections. New families of small molecules that inhibit the assembly and reorganization of the cell wall await discovery (Ha *et al*., 2001; Silver, 2003; Lange *et al*., 2007; Gross *et al*., 2008; van Dam *et al*., 2009); an important step in the development of these compounds is a quantitative, mechanistic understanding of the effect of small molecules on the mechanical properties of the cell wall and their attenuation of cell wall assembly and remodelling (Vollmer, 2006; Vollmer *et al*., 2008; van Dam *et al*., 2009). Given our success in assaying the mechanical effects of A22-mediated MreB disassembly (Fig. 6), CLAMP provides a framework upon which a high-throughput technique may be developed to identify new targets and small molecules that disrupt cell wall assembly and ultimately pathogenesis.

Our work demonstrates how CLAMP can be used to build quantitative relationships between physiological changes and the mechanical properties of the bacterial cell envelope. Deriving physical parameters such as the Young's modulus can have significant impact on our understanding of how cells interact with each other and the surrounding microenvironment, how cells grow and divide and the common features of cell envelope synthesis across different species. In concert with fluorescent labelling, it may also provide insight into the role of intracellular spatiotemporal organization on the assembly of

the cell wall. We anticipate that CLAMP will be particularly useful to microbiologists because it opens a window into viewing the mechanical properties of microbial cell walls, a characteristic that makes this technique particularly useful for building connections among genetics, biochemistry and bacterial cell shape.

Experimental procedures

Preparation of agarose prepolymer

Stock solutions of 5% and 8% w/v UltraPure agarose (Invitrogen Corporation, Carlsbad, CA, USA) were prepared by dissolving agarose in 100 ml of LB medium consisting of tryptone (1% w/v), yeast extract (0.5% w/v) and sodium chloride (1% w/v). The stock solution was autoclaved and stored at 100°C on a heated magnetic stirrer. Working solutions were prepared by mixing LB prewarmed to 65°C with the required volume of the agarose stock solution. We prepared 1–5% (w/v) agarose working solutions from the 5% w/v agarose stock and 6–8% (w/v) agarose working solutions from the 8% agarose stock. The gels were visually homogeneous, with no particulates or deformations observed under high magnification.

Growth of bacterial strains

Individual liquid cultures of *E. coli* MG1655 and *P. aeruginosa* PAO1 were prepared by diluting overnight cultures 1:100 into fresh LB. Liquid cultures of *B. subtilis* BB11 were prepared by diluting an overnight culture 1:100 into fresh LB containing 1 mM IPTG and 0.2 μg ml^{-1} phleomycin. Liquid cultures of *E. coli* FB76 (Bendezú *et al.*, 2009) were prepared by diluting an overnight culture 1:100 into fresh LB containing 25 μg ml^{-1} chloramphenicol. All cultures were grown in a shaker at 37°C with shaking to an absorbance of 0.6 (λ = 600 nm).

Microfluidic flow chamber growth measurements

Cells were grown to an absorbance of 0.1 (λ = 600 nm) in LB, diluted 1:100, and loaded into an ONIX Microfluidic Plate (CellASIC Corporation, Hayward, CA, USA). *B. subtilis* BB11 was grown supplemented with 1 mM IPTG and 0.2 μg ml^{-1} phleomycin. Cells were imaged for 30 min at 30 s intervals using a Nikon Eclipse Ti-E inverted microscope running μManager and equipped with a Nikon Plan Apo 100X objective (numerical aperture of 1.4). To measure whether a change in growth rate occurred when *E. coli* MG1655 cells were treated with A22, cells were seeded into the ONIX chip at an absorbance of 0.001 (λ = 600 nm); after 30 min the medium was switched to LB supplemented with 10 μg ml^{-1} A22, and imaging was continued for an additional 30 min.

Cell length measurements were obtained by using MicrobeTracker (Sliusarenko *et al.*, 2011); fractional extension growth curves and fits were performed using custom MATLAB (The MathWorks, Natick, MA, USA) code. Growth curves that showed unusually large length variation in a single 30 s time step were rejected as a result of probable noise in MicrobeTracker length fitting. Cells that did not grow more than ~ 2% in the first 5 min were also discarded. Strain curves were fit to the exponential function $A \exp(\alpha t)$.

Preparation of polydimethylsiloxane (PDMS) chambers

Polydimethylsiloxane elastomer (Dow Corning, Midland, MI, USA) was prepared at a ratio of 10:1 base : curing agent. We used a spincoater (Laurell Technology Corporation, North Wales, PA, USA) to coat #1.5 glass cover slips with a 250 μm-thick layer of PDMS prepolymer. The PDMS was polymerized by incubating the cover slips for 8–10 h at 65°C. To prepare a chamber for defining the geometry of the agarose gel, we used a scalpel to cut a square 15 mm × 15 mm opening in the centre of the PDMS layer; the height of the chamber was 250 μm.

Encapsulation of live bacterial cells in agarose gels

An aliquot (17 ml) of a log-phase liquid bacterial culture was centrifuged for 5 min at 3000 *g*. We resuspended the resulting cell pellet in 12 ml of LB and centrifuged again for 5 min at 3000 *g*. The resulting cell pellet was resuspended in 200 μl of LB and used for cell encapsulation experiments. Immediately before each experiment, a stock solution of the agarose prepolymer was prepared as described above; from the stock solution, we prepared 10 ml working solutions of agarose and incubated them at 65°C for 5 min to equilibrate. For epifluorescence imaging of strain FB76, the agarose stock solution was made using 1× phosphate-buffered saline rather than LB to reduce background fluorescence. We incubated the working solutions in a 37°C water bath for 1 min prior to the addition of cells. The bacterial cell suspension (200 μl) was incubated at 37°C for 2 min and added to the working solution. Two hundred microlitres of the cell/agarose suspension was poured into a PDMS chamber that was prewarmed to 42°C on a plate heater to ensure that higher-percentage agarose gels did not polymerize instantly. A glass cover slip was pressed against the surface of the PDMS jig and excess molten agarose was forced out, resulting in a 250 μm-thick agarose pad. The gel was incubated on the plate heater for 1 min and then removed and gelled at 25°C. The top glass cover slip was removed from the chamber, the gel was overlaid with LB, the bottom cover slip containing the gel was positioned on the stage of an inverted microscope and the cells were imaged.

Imaging cells

We measured the growth rates of cells encapsulated in agarose gels using phase optics on a TE2000-E + PFS inverted microscope (Nikon, Tokyo, Japan) equipped with a heated stage (Tokai hit, Fujinomiya, Japan), an objective heater (Bioptechs, Butler, PA, USA) and a CoolSNAP DV2 camera (Photometrics, Munich, Germany). The objective heater and heated stage were held at 37°C. We used a Nikon PlanApo 60X oil objective to capture a field of view containing multiple well-separated cells. We imaged cells at focal planes that were ~ 50 μm below the surface of the gel to ensure that cells: (i) were completely encapsulated in agarose and were located far enough from the gel edge to avoid mechanical

effects from the edge of the agarose, (ii) exchanged gas rapidly, which enabled strictly aerobic bacteria such as *B. subtilis* to grow and (iii) were kept in a region of the gel at a constant temperature. We acquired phase contrast images at 1 min intervals over 30 min.

Data analysis

We analysed time-lapse images using MATLAB 2010b (The MathWorks, Inc., Natick, MA, USA) script MicrobeTracker (Sliusarenko *et al.*, 2011) and determined the length of individual cells as a function of time. We manually discarded data from cells that were egregiously out of plane at any stage and growth curves in which errors in cell outline detection led to large, unphysiological jumps in extension. Moreover, small errors in cell length measurements due to out-of-plane growth would not affect our analysis of the *relative* cell length increase $\Delta L/L_0$, since any out-of-plane correction will affect ΔL and L_0 proportionately. The MicrobeTracker parameter file is provided in Table S1. Average growth curves were determined from measurements of 17–51 cells from each species at each agarose concentration.

Measuring the Young's modulus of agarose gels (E_{gel})

Agarose gels (1–8% w/v) were prepared immediately prior to tensile testing and stored in ddH_2O to keep them hydrated; they were prepared as described above without encapsulated cells. Gels were cast in a custom-fabricated mold to comply with the specifications of ASTM D638-03 type IV samples with a gage length of 44.5 mm (ASTM Standard D638, 2003). We used an Instron Model 5548 MicroTester (Instron, Norwood, MA, USA) equipped with a 10 N load cell and custom self-aligning grips to measure the tensile properties of the gels. For each concentration, we measured the mechanical properties of three to nine agarose gels by elongating them at a rate of 10 mm min^{-1} until fracture. Tests were conducted in ambient conditions. Sample cross sections were measured with calipers, and cross head displacement was used to measure extension. E_{gel} was determined by calculating the slope of the linear region of the stress vs. strain response (Figs S1 and S2).

Rate of growth of E. coli *cells on agarose surfaces*

To determine whether cell contact with agarose influenced cell growth, we measured the growth rate of *E. coli* MG1655 on gel surfaces. Cells were cultured and prepared as described above, and a 5 µl aliquot was transferred onto the surfaces of 1%, 3% and 5% w/v agarose gels. We inverted the gels onto a glass cover slip and imaged cell growth at 1 min intervals for 60 min at 37°C. The elongation rate was determined using MicrobeTracker, and the doubling time was determined from data for individual cells; average growth curves were essentially independent of gel stiffness (Fig. S3).

Metabolic activity of bacteria encapsulated in agarose gels

We used the redox indicator 5-cyano-2,3-ditolyltetrazolium chloride (CTC) to measure the metabolic activity of *E. coli* MG1655 cells encapsulated in gels (5% w/v) in which the mechanical resistance of the gel to cell growth was large. Following encapsulation, the gels were overlaid with 200 µl of LB and incubated at 37°C. After 0, 30, 60 and 90 min of incubation, we removed the LB from the gel surface and overlaid a solution of 25 mM CTC on top of the agarose. We incubated for 30 min to allow the CTC to diffuse through the gel, after which the equilibrium concentration of CTC in the gel was 50 µM. We then imaged cells using epifluorescence microscopy ($\lambda_{excitation}$ = 484 nm; $\lambda_{emission}$ = 620 nm) on a Nikon TE2000 inverted microscope using an Andor iXon EMCCD (Belfast, Northern Ireland). As a negative control, we killed *E. coli* MG1655 cells by exposing them to 80% ethanol for 15 min, added CTC to a final concentration of 50 µM, incubated for 30 min, transferred the cells to an agarose pad, and imaged using phase contrast and epifluorescence microscopy. CTC did not label these cells (Fig. S4).

Effect of A22 on the mechanical properties of E. coli *cells*

We determined the effect of MreB depolymerization on *E. coli* MG1655 stiffness by adding S-(3,4-dichlorobenzyl) isothiourea (A22) to the agarose during cell encapsulation; the compound was synthesized according to published procedures and recrystallized three times (Iwai *et al.*, 2004). Cells and agarose working solutions were prepared as described, except that during the preparation of the agarose working solution, A22 was added to the LB to a final concentration in the gel of 10 µg ml^{-1}. The encapsulation of cells in agarose containing A22 caused rapid delocalization of MreB (Fig. S8).

Computational methods

Using the finite-element analysis software COMSOL 4.2 (COMSOL, Inc., Burlington, MA, USA), we represented a cell as a thin cylindrical shell with hemispherical endcaps. The thickness of the shell was 30 nm and the cylinder had a radius of 0.5 µm and a length of 4 µm for *E. coli* and *P. aeruginosa* or 8 µm for *B. subtilis*. For *E. coli* and *P. aeruginosa*, E_{cell} was scaled by a factor of 4/30 to mimic the surface modulus of a shell with thickness 4 nm. We set the Young's modulus of the endcaps to 1000 MPa to focus on the elongation of the cylindrical region. The surrounding gel was a cylindrical volume 50 µm in length along the long axis of the cell and 20 µm in diameter along the other two dimensions. E_{gel} was varied according to the gel moduli in Fig. S1, while E_{cell} was varied from 10 to 250 MPa. Most rigid polymers have a Poisson ratio between 0.3 and 0.5 (Simmons and Wang, 1971), thus we assumed a Poisson ratio of $\nu = 0.4$ for all 3D simulations; the precise value of ν has little effect on our results. To mimic elongation of the cylindrical body, the rest length of the cylinder was increased by 1%. After the cell and gel relaxed to a new mechanical equilibrium, the length of the cell was measured to compute the relative extension $\Delta L/L_0$.

Acknowledgements

We thank Gaurav Misra for helpful conversations, Tom Record for use of a vapor pressure osmometer, Piet de Boer

for *E. coli* strain FB76 and Rut Carballido-Lopez for *B. subtilis* strain BB11. We acknowledge the Aspen Center for Physics and NSF grant 1066293. H. H. T. acknowledges support from an NIH National Research Service Award (T32 GM07215). C. T. acknowledges support from a Stanford Graduate Fellowship and the Bruce and Elizabeth Dunlevie Bio-X Stanford Interdisciplinary Graduate Fellowship. K. C. H. acknowledges support from a National Institutes of Health K25 award (5K25 GM075000) and an NIH Director's New Innovator award (DP2OD006466). K. C. H. and A. G. acknowledge support from NSF grant EF-1038697. A. G. acknowledges support from the James S. McDonnell Foundation. D. B. W. acknowledges support from DuPont, the Alfred P. Sloan Foundation and an NIH Director's New Innovator award (DP2OD008735).

References

Abu-Lail, N.I., and Camesano, T.A. (2006) The effect of solvent polarity on the molecular surface properties and adhesion of *Escherichia coli*. *Colloids Surf B Biointerfaces* **51:** 62–70.

ASTM Standard D638 (2003) *Standard Test Method for Tensile Properties of Plastics*. West Conshohocken, PA: ASTM International, doi:10.1520/D0638-03 [WWW document]. URL: http://www.astm.org.

Bashan, Y., and Gonzalez, L. (1999) Long-term survival of the plant-growth-promoting bacteria *Azospirillum brasilense* and *Pseudomonas fluorescens* in dry alginate inoculant. *Appl Microbiol Biotechnol* **51:** 262–266.

Bean, G.J., Flickinger, S.T., Westler, W.M., McCully, M.E., Sept, D., Weibel, D.B., and Amann, K.J. (2009) A22 disrupts the bacterial actin cytoskeleton by directly binding and inducing a low-affinity state in MreB. *Biochemistry* **48:** 4852–4857.

Bendezú, F.O., Hale, C.A., Bernhardt, T.G., and de Boer, P.A.J. (2009) RodZ (YfgA) is required for proper assembly of the MreB actin cytoskeleton and cell shape in *E. coli*. *EMBO J* **28:** 193–204.

Ben-Dov, E., Kramarsky-Winter, E., and Kushmaro, A. (2009) An in situ method for cultivating microorganisms using a double encapsulation technique. *FEMS Microbiol Ecol* **68:** 363–371.

Boulbitch, A., Quinn, B., and Pink, D. (2000) Elasticity of the rod-shaped Gram-negative Eubacteria. *Phys Rev Lett* **85:** 5246–5249.

Carballido-Lopez, R., and Formstone, A. (2007) Shape determination in *Bacillus subtilis*. *Curr Opin Microbiol* **10:** 611–616.

Cerf, A., Cau, J.-C., Vieu, C., and Dague, E. (2009) Nanomechanical properties of dead or alive single-patterned bacteria. *Langmuir* **25:** 5731–5736.

Chen, Y.-Y., Wu, C.-C., Hsu, J.-L., Peng, H.-L., Chang, H.-Y., and Yew, T.-R. (2009) Surface rigidity change of *Escherichia coli* after filamentous bacteriophage infection. *Langmuir* **25:** 4607–4614.

van Dam, V., Olrichs, N., and Breukink, E. (2009) Specific labeling of peptidoglycan precursors as a tool for bacterial cell wall studies. *Chembiochem* **10:** 617–624.

Defeu Soufo, H.J., Reimold, C., Linne, U., Knust, T., Gescher, J., and Graumann, P.L. (2010) Bacterial translation elongation factor EF-Tu interacts and colocalizes with actin-like MreB protein. *Proc Natl Acad Sci USA* **107:** 3163–3168.

Deng, Y., Sun, M., and Shaevitz, J.W. (2011) Direct measurement of cell wall stress stiffening and turgor pressure in live bacterial cells. *Phys Rev Lett* **107:** 158101.

Eaton, P., Fernandes, J.C., Pereira, E., Pintado, M.E., and Malcata, F.X. (2008) Atomic force microscopy study of the antibacterial effects of chitosans on *Escherichia coli* and *Staphylococcus aureus*. *Ultramicroscopy* **108:** 1128–1134.

Eun, Y.-J., Utada, A.S., Copeland, M.F., Takeuchi, S., and Weibel, D.B. (2011) Encapsulating bacteria in agarose microparticles using microfluidics for high-throughput cell analysis and isolation. *ACS Chem Biol* **6:** 260–266.

Flemming, C.A., Leung, K.T., Lee, H., Trevors, J.T., and Greer, C.W. (1994) Survival of *lux-lac*-marked biosurfactant-producing *Pseudomonas aeruginosa* UG2L in soil monitored by nonselective plating and PCR. *Appl Environ Microbiol* **60:** 1606–1613.

Francius, G., Domenech, O., Mingeot-Leclercq, M.P., and Dufrene, Y.F. (2008) Direct observation of *Staphylococcus aureus* cell wall digestion by lysostaphin. *J Bacteriol* **190:** 7904–7909.

Furchtgott, L., Wingreen, N.S., and Huang, K.C. (2011) Mechanisms for maintaining cell shape in rod-shaped Gram-negative bacteria. *Mol Microbiol* **81:** 340–353.

Gaboriaud, F., Bailet, S., Dague, E., and Jorand, F. (2005) Surface structure and nanomechanical properties of *Shewanella putrefaciens* bacteria at two pH values (4 and 10) determined by atomic force microscopy. *J Bacteriol* **187:** 3864–3868.

Gaboriaud, F., Parcha, B.S., Gee, M.L., Holden, J.A., and Strugnell, R.A. (2008) Spatially resolved force spectroscopy of bacterial surfaces using force-volume imaging. *Colloids Surf B Biointerfaces* **62:** 206–213.

Gan, L., Chen, S., and Jensen, G.J. (2008) Molecular organization of Gram-negative peptidoglycan. *Proc Natl Acad Sci USA* **105:** 18953–18957.

Gift, E.A., Park, H.J., Paradis, G.A., Demain, A.L., and Weaver, J.C. (1996) FACS-based isolation of slowly growing cells: double encapsulation of yeast in gel microdrops. *Nat Biotechnol* **14:** 884–887.

Gitai, Z., Dye, N., and Shapiro, L. (2004) An actin-like gene can determine cell polarity in bacteria. *Proc Natl Acad Sci USA* **101:** 8643–8648.

Gitai, Z., Dye, N.A., Reisenauer, A., Wachi, M., and Shapiro, L. (2005) MreB actin-mediated segregation of a specific region of a bacterial chromosome. *Cell* **120:** 329–341.

Gross, B.J., Swoboda, J.G., and Walker, S. (2008) A strategy to discover inhibitors of O-linked glycosylation. *J Am Chem Soc* **130:** 440–441.

Ha, S., Gross, B., and Walker, S. (2001) *E. coli* MurG: a paradigm for a superfamily of glycosyltransferases. *Curr Drug Targets Infect Disord* **1:** 201–213.

Hayhurst, E.J., Kailas, L., Hobbs, J.K., and Foster, S.J. (2008) Cell wall peptidoglycan architecture in *Bacillus subtilis*. *Proc Natl Acad Sci USA* **105:** 14603–14608.

Hobot, J.A., Carlemalm, E., Villiger, W., and Kellenberger, E. (1984) Periplasmic gel: new concept resulting from the reinvestigation of bacterial cell envelope ultrastructure by new methods. *J Bacteriol* **160:** 143–152.

Holtje, J.V. (1998) Growth of the stress-bearing and shape-

maintaining murein sacculus of *Escherichia coli*. *Microbiol Mol Biol Rev* **62:** 181–203.

Huang, K.C., Mukhopadhyay, R., Wen, B., Gitai, Z., and Wingreen, N.S. (2008) Cell shape and cell-wall organization in Gram-negative bacteria. *Proc Natl Acad Sci USA* **105:** 19282–19287.

Iwai, N., Nagai, K., and Wachi, M. (2002) Novel S-benzylisothiourea compound that induces spherical cells in *Escherichia coli* probably by acting on a rod-shape-determining protein(s) other than penicillin-binding protein 2. *Biosci Biotechnol Biochem* **66:** 2658–2662.

Iwai, N., Ebata, T., Nagura, H., Kitazume, T., Nagai, K., and Wachi, M. (2004) Structure-activity relationship of S-benzylisothiourea derivatives to induce spherical cells in *Escherichia coli*. *Biosci Biotechnol Biochem* **68:** 2265–2269.

Jain, R., Saxena, J., and Sharma, V. (2010) The evaluation of free and encapsulated *Aspergillus awamori* for phosphate solubilization in fermentation and soil-plant system. *Appl Soil Ecol* **46:** 90–94.

Katsuragi, T., Tanaka, S., Nagahiro, S., and Tani, Y. (2000) Gel microdroplet technique leaving microorganisms alive for sorting by flow cytometry. *J Microbiol Methods* **42:** 81–86.

Kruse, T., Bork-Jensen, J., and Gerdes, K. (2005) The morphogenetic MreBCD proteins of *Escherichia coli* form an essential membrane-bound complex. *Mol Microbiol* **55:** 78–89.

Kumar, U., Vivekanand, K., and Poddar, P. (2009) Real-time nanomechanical and topographical mapping on live bacterial cells – *Brevibacterium casei* under stress due to their exposure to Co^{2+} ions during microbial synthesis of Co_3O_4 nanoparticles. *J Phys Chem B* **113:** 7927–7933.

Lange, R.P., Locher, H.H., Wyss, P.C., and Then, R.L. (2007) The targets of currently used antibacterial agents: lessons for drug discovery. *Curr Pharm Des* **13:** 3140–3154.

Matias, V.R.F., and Beveridge, T.J. (2005) Cryo-electron microscopy reveals native polymeric cell wall structure in *Bacillus subtilis* 168 and the existence of a periplasmic space. *Mol Microbiol* **56:** 240–251.

Matias, V.R.F., and Beveridge, T.J. (2008) Lipoteichoic acid is a major component of the *Bacillus subtilis* periplasm. *J Bacteriol* **190:** 7414–7418.

Minc, N., Boudaoud, A., and Chang, F. (2009) Mechanical forces of fission yeast growth. *Curr Biol* **19:** 1096–1101.

Nilsen, T., Ghosh, A.S., Goldberg, M.B., and Young, K.D. (2004) Branching sites and morphological abnormalities behave as ectopic poles in shape-defective *Escherichia coli*. *Mol Microbiol* **52:** 1045–1054.

Penegar, I., Toque, C., Connell, S.D.A., Smith, J.R., and Campbell, S.A. (1999) Nano-indentation measurements of the marine bacteria *Sphingomonas paucimobilis* using the atomic force microscope. In *10th International Congress on Marine Corrosion and Fouling*. Lewis, J.A. (ed.). Melbourne: DSTO Aeronautical and Maritime Research Laboratory, pp. 5–15.

Perry, C.C., Weatherly, M., Beale, T., and Randriamahefa, A. (2009) Atomic force microscopy study of the antimicrobial activity of aqueous garlic versus ampicillin against *Escherichia coli* and *Staphylococcus aureus*. *J Sci Food Agric* **89:** 958–964.

Popham, D.L., and Young, K.D. (2003) Role of penicillin-binding proteins in bacterial cell morphogenesis. *Curr Opin Microbiol* **6:** 594–599.

Sabass, B., Gardel, M.L., Waterman, C.M., and Schwarz, U.S. (2008) High resolution traction force microscopy based on experimental and computational advances. *Biophys J* **94:** 207–220.

Silver, L.L. (2003) Novel inhibitors of bacterial cell wall synthesis. *Curr Opin Microbiol* **6:** 431–438.

Simmons, G., and Wang, H. (1971) *Single Crystal Elastic Constants and Calculated Aggregate Properties: A Handbook*. p. xv, 370 pp. Cambridge, MA: MIT Press.

Sliusarenko, O., Heinritz, J., Emonet, T., and Jacobs-Wagner, C. (2011) High-throughput, subpixel precision analysis of bacterial morphogenesis and intracellular spatio-temporal dynamics. *Mol Microbiol* **80:** 612–627.

van Teeffelen, S., Wang, S., Furchtgott, L., Huang, K.C., Wingreen, N.S., Shaevitz, J.W., and Gitai, Z. (2011) The bacterial actin MreB rotates, and rotation depends on cell-wall assembly. *Proc Natl Acad Sci USA* **108:** 15822–15827.

Thwaites, J.J., and Mendelson, N.H. (1989) Mechanical properties of peptidoglycan as determined from bacterial thread. *Int J Biol Macromol* **11:** 201–206.

Thwaites, J.J., and Mendelson, N.H. (1991) Mechanical behavior of bacterial cell walls. *Adv Microb Physiol* **32:** 173–222.

Thwaites, J.J., and Surana, U.C. (1991) Mechanical properties of *Bacillus subtilis* cell walls: effects of removing residual culture medium. *J Bacteriol* **173:** 197–203.

Vadillo-Rodriguez, V., Beveridge, T.J., and Dutcher, J.R. (2008) Surface viscoelasticity of individual Gram-negative bacterial cells measured using atomic force microscopy. *J Bacteriol* **190:** 4225–4232.

Varma, A., and Young, K.D. (2004) FtsZ collaborates with penicillin binding proteins to generate bacterial cell shape in *Escherichia coli*. *J Bacteriol* **186:** 6768–6774.

Vollmer, W. (2006) The prokaryotic cytoskeleton: a putative target for inhibitors and antibiotics? *Appl Microbiol Biotechnol* **73:** 37–47.

Vollmer, W., and Bertsche, U. (2008) Murein (peptidoglycan) structure, architecture and biosynthesis in *Escherichia coli*. *Biochim Biophys Acta* **1778:** 1714–1734.

Vollmer, W., Blanot, D., and de Pedro, M.A. (2008) Peptidoglycan structure and architecture. *FEMS Microbiol Rev* **32:** 149–167.

Wang, J.H.-C., and Lin, J.-S. (2007) Cell traction force and measurement methods. *Biomech Model Mechanobiol* **6:** 361–371.

Wang, S., Arellano-Santoyo, H., Combs, P.A., and Shaevitz, J.W. (2010) Actin-like cytoskeleton filaments contribute to cell mechanics in bacteria. *Proc Natl Acad Sci USA* **107:** 9182–9185.

Xu, W., Mulhern, P.J., Blackford, B.L., Jericho, M.H., Firtel, M., and Beveridge, T.J. (1996) Modeling and measuring the elastic properties of an archaeal surface, the sheath of *Methanospirillum hungatei*, and the implication for methane production. *J Bacteriol* **178:** 3106–3112.

Yao, X., Jericho, M., Pink, D., and Beveridge, T. (1999) Thickness and elasticity of gram-negative murein sacculi measured by atomic force microscopy. *J Bacteriol* **181:** 6865–6875.

Young, C.-C., Rekha, P.D., Lai, W.-A., and Arun, A.B. (2006) Encapsulation of plant growth-promoting bacteria in alginate beads enriched with humic acid. *Biotechnol Bioeng* **95:** 76–83.

Zengler, K., Toledo, G., Rappe, M., Elkins, J., Mathur, E.J., Short, J.M., and Keller, M. (2002) Cultivating the uncultured. *Proc Natl Acad Sci USA* **99:** 15681–15686.

Zienkewicz, O.C. (2005) *The Finite Element Method for Solid and Structural Mechanics*. Oxford: Butterworth-Heinemann.

Supporting information

Additional supporting information may be found in the online version of this article.

Please note: Wiley-Blackwell are not responsible for the content or functionality of any supporting materials supplied by the authors. Any queries (other than missing material) should be directed to the corresponding author for the article.